

Intelligent Reflecting Surface for Multicell MIMO Communications

Cunhua Pan, Hong Ren, Kezhi Wang, Wei Xu, Maged El Kashlan, Arumugam Nallanathan, *Fellow, IEEE*, and Lajos Hanzo, *Fellow, IEEE*

Abstract

Intelligent reflecting surface (IRS) is envisioned to be a disruptive and revolutionizing technology that can achieve both spectral and energy efficient wireless communications as well as provide a radio-controllable environment. In specific, IRS is a planar that consists of a large number of passive reflection elements that induce phase shifts on the impinging electromagnetic waves so that the reflected signal can be constructively added at the desired user or destructively at the unintended users. In this paper, we propose to deploy an IRS at cell boundary of multiple cells to assist the transmission for cell-edge users, and also help alleviate the inter-cell interference, which is a crucial issue in multicell communication systems. We aim to maximize the weighted sum rate (WSR) of all users through jointly optimizing the active precoding matrices at the base stations (BSs) and the phase shifts at the IRS subject to each BS's power constraint and unit modulus constraint. Both BSs and users are equipped with multiple antennas, which can enhance the spectral efficiency. Due to the non-convexity of the problem, we first reformulate it into an equivalent one, which is solved by using the block coordinate descent (BCD) algorithm where precoding matrices and phase shifts are alternatively optimized. The optimal precoding matrices can be obtained in closed form when fixing the phase shifts. Two efficient algorithms are proposed to solve the phase shift optimization problem, i.e., Majorization-Minimization (MM) Algorithm and Complex Circle Manifold (CCM) Method. Both algorithms are guaranteed to converge to at least locally optimal solution. Finally, simulation results confirm the advantages of introducing IRS in enhancing the cell-edge user performance.

I. INTRODUCTION

The forthcoming fifth-generation (5G) and beyond wireless communication system is expected to provide a 1000-fold increase in the network capacity over current 4G system due to the

C. Pan, H. Ren, M. El Kashlan and A. Nallanathan are with the School of Electronic Engineering and Computer Science at Queen Mary University of London, London E1 4NS, U.K. (e-mail: {c.pan, h.ren, maged.elkashlan, a.nallanathan}@qmul.ac.uk). K. Wang is with Department of Computer and Information Sciences, Northumbria University, UK. (e-mail: kezhi.wang@northumbria.ac.uk). W. Xu is with National Mobile Communications Research Laboratory, Southeast University, Nanjing 210096, China. (e-mail: wxu@seu.edu.cn). L. Hanzo is with the School of Electronics and Computer Science, University of Southampton, Southampton, SO17 1BJ, U.K. (e-mail: lh@ecs.soton.ac.uk).

ever-increasing demand for higher data rates requirement driven by some emerging applications such as augmented reality (AR) and virtual reality (VR). To achieve this goal, some promising techniques are proposed such as massive multiple-input multiple-output (MIMO) [1], millimeter wave (mmWave) communications [2], and ultra-dense cloud radio access networks (UD-CRAN) [3], [4]. By deploying a massive number of antennas at the base station (BS) and transmission over the millimeter-wave (mm-wave) bands, significant spectral efficiency improvement can be achieved by exploiting spatial multiplexing gain and high frequency band. However, excessive signal processing complexity, increased hardware cost as well as high power consumption are incurred when installing more antenna elements and operating radio frequency (RF) chains in high frequency band. These issues restrict their wide and practical deployment in 5G systems. Although the access points (AP) can be densely deployed in UD-CRAN to reduce the access distance between users and APs, limited fronthaul capacity constitutes a performance bottleneck. Furthermore, these techniques only focus on the transceiver design to cater to the dynamic wireless channels, and the unfavourable electromagnetic wave propagation such as blockage or deep fading cannot be controlled.

Motivated by above, intelligent reflecting surface (IRS) has been proposed as an innovative and revolutionizing technique to enable both spectrum and energy efficient communications through reconfiguring the wireless propagation environment [5], [6]. In specific, an IRS consists of a vast number of low-cost passive reflecting elements, each of which can independently adjust its phase shift of the incident signals, and thus collaboratively alter the reflected signal propagation to create favourable wireless transmission channels. By properly tuning the phase shifts by using an IRS controller, the reflected signals can be added constructively at the desired receiver to enhance the received signal power or destructively at non-intended receivers to reduce the co-channel interference. Although passive reflecting surfaces have been used in radar systems, the phase shifts of passive elements cannot be changed once fabricated, and thus cannot control the wireless propagation channels. Fortunately, due to the recent development in micro electromechanical systems (MEMS) and metamaterial [7], the phase shifts can be adjusted in real time, which makes IRS possible. Although IRS resembles the amplify-and-forward (AF) relay, the former has the advantage of lower power consumption since it only reflects the signals passively without RF chains while the latter requires active RF components for signal transmission. Hence, IRS does not introduce additional thermal noise at the reflected signals. Due to low functionalities, the phase

shifts can be fabricated in small size. Then, each IRS can be packed with a large number of phase shifters and provide high beamforming gain. Furthermore, IRSs possess the appealing advantages of light weight and small sizes, which can be easily installed in buildings facades, ceilings, lamp poles, road signs, etc. IRSs can also be integrated into the existing communication systems with a minor modification of their communication standardization and hardware. However, to reap the aforementioned benefits promised by IRSs, the phase shifts should be properly optimized along with the active beamforming at BS. The main difficulty in optimizing the phase shifts is the non-convex unit modulus constraint. Although this kind of constraints has been studied in hybrid digital/analog precoding [8], [9] and constant-envelope precoding in massive MIMO [10], [11]. However, they only focus on the designs at the transmitter, which are not applicable for the joint active beamforming design at BSs and passive beamforming design at IRS.

Most recently, there are some initial efforts devoted to the transmission design for IRS-assisted wireless communication systems, such as single-user case in [12]–[15], downlink multiuser case in [16]–[20], and physical layer security in [21]–[24]. Specifically, received signal power maximization problem was studied in [12], where semidefinite relaxation (SDR) was employed to solve the problem. It is widely known that SDR method has higher computational complexity. To reduce its complexity, Yu *et al.* proposed two efficient fixed point iteration and manifold optimization techniques to solve the same problem as in [12]. Sum rate maximization problem was considered in IRS-enhanced orthogonal frequency division multiplexing (OFDM) system by jointly optimizing the power allocation and phase shifts. Successive convex approximation (SCA) technique was introduced to find the optimal phase shifts. The authors in [15] derived the closed-form expression of the phase shifts when only statistical channel state information (CSI) is available. For multiuser case, reference [16] aimed at minimizing the total transmit power while guaranteeing each user's signal-to-interference-plus-noise ratio (SINR) constraints. Two approximate solutions based on the SDR and alternating optimization techniques were developed to solve this problem. Huang *et al.* [17] investigated the sum rate/energy efficiency maximization problem, where the BS employs zero-forcing (ZF) transmission, and the phase shifts were optimized by using gradient descent search and sequential fractional programming. This work shows that the IRS-assisted system is more energy-efficient than a traditional relay-assisted communication system. The weighted sum rate maximization was studied in [18], where the fractional programming method was used to find the active beamforming at BS, and three efficient algorithms were developed to optimize

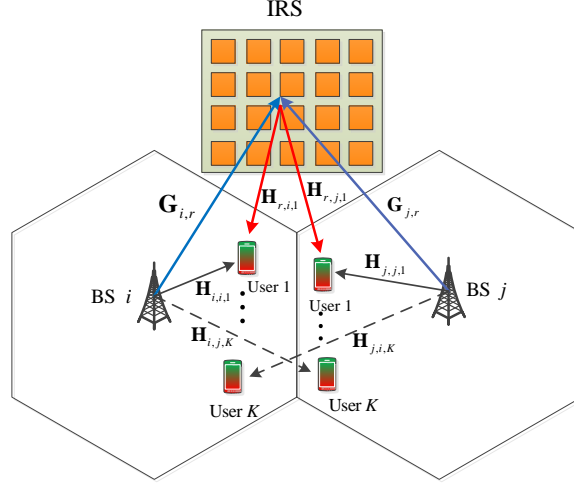


Fig. 1. An IRS-assisted multicell MIMO multiuser communication system.

the phase shifts. The large system analysis was employed to derive the closed-form expression of the minimum SINR in [19] when only spatial correlation matrices for the IRS elements are available. Then, the authors targeted at maximizing the minimum SINR by optimizing the phase shifts based on the derived expression. Compressive sensing and deep learning methods were developed in [20] for the challenging channel estimation task in LIS-assisted systems. The secrecy rate maximization problem was studied in [21]–[23] with only one legitimate receiver and one eavesdropper, and various algorithms were proposed to solve the same optimization problem, i.e., element-wise optimization and alternating optimization in [21], Charnes-Cooper transformation and SDR in [22], and alternating algorithm combined with bisection search method in [23]. Most recently, Chen *et al.* [24] considered the more general scenario with multiple legitimate receivers and multiple eavesdroppers. One iterative algorithm based on the alternating optimization and the path-following algorithm was proposed to solve the non-convex optimization problem.

However, the above-mentioned papers only studied the single-cell case, and the multicell case is still lack of investigation in existing literature. To deal with the spectrum scarcity issue, different cells will reuse the same frequency resource, which causes the severe inter-cell interference, especially for cell-edge users [25]. In this paper, we propose to deploy an IRS at the cell boundary to assist the transmission for cell-edge users in multicell systems as shown in Fig. 1, where the inter-cell interference can be alleviated with the aid of IRS. Specifically, by carefully adjusting the phase shifts of the IRS's reflection elements, the inter-cell interference reflected by the IRS can be added

destructively with the direct interference from the adjacent BS to minimize interference power at receivers. This provides more degrees of freedom for designing the beamforming/precoding at each BS for users in its own cell. As a result, both active beamforming/precoding at each BS and passive beamforming at the IRS should be jointly optimized. This kind of optimization problem is difficult to solve as the optimization variables are highly coupled. Furthermore, all the existing contributions consider the single-antenna user case. Due to the rapid development in antenna technology [26], the user equipment can be packed with multiple antennas to enhance the received signal strength. Then, multiple data streams can be transmitted simultaneously, which boost the spectral efficiency. Therefore, in this paper, we consider the multiple-antenna user case. Due to the complicated expression associated with the data rate expression, the existing techniques in [12]–[24] cannot be directly applied. The multiple-antenna user case additionally complicates the optimization.

The main contributions of this paper can be summarized as follows:

- 1) To the best of our knowledge, this is the first attempt to explore the assistance of IRS to enhance the cell-edge user performance for multicell MIMO communication systems. In specific, we jointly optimize the active precoding matrices from all BSs and phase shifts at the IRS to maximize the weighted sum rate (WSR) of all users subject to each BS's power constraint and unit modulus constraint for the phase shifters. However, the objective function is not jointly concave over both precoding matrices and phase shifts, which are highly coupled. To tackle this difficult problem, we first reformulate the original problem into its equivalent one by exploiting the equivalence between data rate and weighted minimum mean-square error (WMMSE). Then, the block coordinate descent (BCD) algorithm is proposed to alternatively optimize precoding matrices at BSs and passive beamforming at IRS.
- 2) Given fixed phase shifts, we derive the optimal precoding matrices in closed form by applying Lagrangian multiplier method. For the difficult phase shift optimization problem, it is highly coupled with various channel matrices and precoding matrices. By using some matrix manipulations and transformations, we successfully transform the phase shift optimization problem into a non-convex quadratically constrained quadratic program (QCQP) with unit modulus constraint. Two efficient iterative algorithms are proposed for solving this problem. The first one is Majorization-Minimization (MM) Algorithm, where the closed-form solution can be obtained in each iteration. The second is based on Complex Circle Manifold (CCM) Method,

where we show that unit modulus constraints of all phase shifters constitute a complex circle manifold. Both the MM algorithm and CCM algorithm are guaranteed to converge to at least locally optimal solution.

- 3) Simulation results show that the cell-edge user performance can be significantly enhanced by deploying an IRS compared with the conventional multicell system without an IRS. Moreover, it is also shown that the performance gain achieved by the IRS is mainly due to the favourable channel link related to IRS, i.e., BS-IRS link and IRS-user link. Furthermore, the location of IRS should be carefully deployed. It is suggested that deploying at the cell boundary can achieve largest gains for cell-edge users. It is a promising result as the reflected signals by the passive device is weak, and should be deployed in the vicinity of users.

The remainder of this paper is organized as follows. In Section II, we present the system model of the IRS-assisted multicell MIMO communication and formulate the WSR maximization problem. In Section III, we reformulate the original problem into a more tractable problem and both active precoding matrices and passive beamforming are alternatively optimized. In Section IV, extensive simulation results are provided to demonstrate the performance advantages of introducing an IRS into multicell systems. Finally, our conclusions are drawn in Section V.

Notations: For a complex value a , $\text{Re}\{a\}$ represents the real part of a . Boldface lower case and upper case letters denote vectors and matrices, respectively. \mathbb{C}^M denotes the set of $M \times 1$ complex vectors. $\mathbb{E}\{\cdot\}$ denotes the expectation operation. $\|\mathbf{x}\|_2$ denotes the 2-norm of vector \mathbf{x} . For two matrices \mathbf{A} and \mathbf{B} , $\mathbf{A} \odot \mathbf{B}$ represents Hadamard product of \mathbf{A} and \mathbf{B} . $\|\mathbf{A}\|_F$, $\text{Tr}(\mathbf{A})$ and $|\mathbf{A}|$ denote the Frobenius norm, trace operation and determinant of \mathbf{A} , respectively. $\nabla f_{\mathbf{x}}(\mathbf{x})$ denotes the gradient of the function f with respect to (w.r.t.) the vector \mathbf{x} . $\mathcal{CN}(\mathbf{0}, \mathbf{I})$ represents a random vector following the distribution of zero mean and unit variance matrix. $\arg\{\cdot\}$ means the extraction of phase information. $\text{diag}(\cdot)$ denotes the diagonalization operation. $(\cdot)^*$, $(\cdot)^T$ and $(\cdot)^H$ denote the conjugate, transpose and Hermitian operators, respectively.

II. SYSTEM MODEL AND PROBLEM FORMULATION

A. System Model

We consider an IRS-aided downlink multicell MIMO system model with L macro cells, each of which has only one base station (BS) that serves K cell-edge users. Each BS and each user are equipped with N_t and N_r antennas, respectively. For each cell-edge user, it suffers both high

signal attenuation from its serving cell and severe cochannel interference from its neighbouring BSs. To resolve this issue, we propose to deploy an IRS which has M reflection elements at the cell edge as shown in Fig. 1, which can help enhance the useful signal power and control the cochannel interference by carefully designing its reflecting phase shifts.

The transmit signal at the l th BS is given by

$$\mathbf{x}_l = \sum_{k=1}^K \mathbf{F}_{l,k} \mathbf{s}_{l,k} \quad (1)$$

where $\mathbf{s}_{l,k}$ is the $d \times 1$ transmitted data symbol vector for the k th user in its cell, satisfying $\mathbb{E}[\mathbf{s}_{l,k} \mathbf{s}_{l,k}^H] = \mathbf{I}_d$ and $\mathbb{E}[\mathbf{s}_{l,k} (\mathbf{s}_{i,j})^H] = \mathbf{0}$, for $\{l, k\} \neq \{i, j\}$, $\mathbf{F}_{l,k} \in \mathbb{C}^{N_t \times d}$ is the linear precoding matrix used by the l th BS to transmit data vector $\mathbf{s}_{l,k}$ to the k th user. The baseband channels from the i th BS to the k th user in the l th cell, from the IRS to the k th user in the l th cell, from the i th BS to the IRS are denoted as $\mathbf{H}_{i,l,k}$, $\mathbf{H}_{r,l,k}$ and $\mathbf{G}_{i,r}$, respectively. Denote $\theta_m \in [0, 2\pi]$ as the the phase shift of the m -th reflection element of the IRS, and thus the reflection operator is to multiply the incident multi-path signals with $e^{j\theta_m}$ ¹ at a single physical point, and then forward the combined signal to the users. Hence, the users will not only receive the signals from the BSs, but also the signals from the IRS. In addition, we ignore the signal power that has been reflected two or more times due to severe path loss. Let us denote the diagonal phase-shifting matrix of the IRS as $\Phi = \text{diag}\{e^{j\theta_1}, \dots, e^{j\theta_m}, \dots, e^{j\theta_M}\}$, the received signal vector at the k th user in the l th cell is given by

$$\mathbf{y}_{l,k} = \underbrace{\sum_{n=1}^L \mathbf{H}_{n,l,k} \mathbf{x}_n}_{\text{Signals from BSs}} + \underbrace{\sum_{n=1}^L \mathbf{H}_{r,l,k} \Phi \mathbf{G}_{n,r} \mathbf{x}_n}_{\text{Signals from the IRS}} + \mathbf{n}_{l,k}, \quad (2)$$

where $\mathbf{n}_{l,k}$ is the noise vector that satisfies $\mathcal{CN}(\mathbf{0}, \sigma^2 \mathbf{I}_{N_r})$.

In this paper, we assume that the channel state information for all channels are perfectly available at the BS, and the BS calculates the optimal phase shifts and sends back to the IRS controller. It should be emphasized that the assumption of perfect CSI knowledge at the BS is idealistic, and it is challenging to obtain the CSI in IRS-assisted communication system. However, the proposed algorithms developed in this paper can serve as the performance upper bound for realistic scenarios with the channel estimation error. In addition, the proposed algorithms can provide some insights on the performance gain brought by the IRS, which can motivate more research efforts in this area.

¹ j is the imaginary unit.

Please note that there are a few papers studying the channel estimation for IRS-assisted systems, such as compressive sensing and deep learning method in [20].

Define $\bar{\mathbf{H}}_{n,l,k} \triangleq \mathbf{H}_{r,l,k} \Phi \mathbf{G}_{n,r} + \mathbf{H}_{n,l,k}$, which can be regarded as the equivalent channel from the n th BS to the k th user in the l th cell. By substituting (1) into (2), $\mathbf{y}_{l,k}$ can be rewritten as

$$\mathbf{y}_{l,k} = \underbrace{\bar{\mathbf{H}}_{l,l,k} \mathbf{F}_{l,k} \mathbf{s}_{l,k}}_{\text{Intra-cell interference}} + \underbrace{\sum_{n=1, n \neq l}^L \sum_{m=1}^K \bar{\mathbf{H}}_{n,l,k} \mathbf{F}_{n,m} \mathbf{s}_{n,m}}_{\text{Inter-cell interference}} + \mathbf{n}_{l,k}. \quad (3)$$

Then, the achievable data rate (nat/s/Hz) of the k th user in the l th cell is given by [27]

$$R_{l,k}(\mathbf{F}, \boldsymbol{\theta}) = \log \left| \mathbf{I} + \bar{\mathbf{H}}_{l,l,k} \mathbf{F}_{l,k} \mathbf{F}_{l,k}^H \bar{\mathbf{H}}_{l,l,k}^H \mathbf{J}_{l,k}^{-1} \right|, \quad (4)$$

where $\mathbf{F} = [\mathbf{F}_{l,k}, \forall l, k]$, $\boldsymbol{\theta} = [\theta_1, \dots, \theta_M]$, and $\mathbf{J}_{l,k}$ the interference-plus-noise covariance matrix given by

$$\mathbf{J}_{l,k} = \sum_{m=1, m \neq k}^K \bar{\mathbf{H}}_{l,l,k} \mathbf{F}_{l,m} \mathbf{F}_{l,m}^H \bar{\mathbf{H}}_{l,l,k}^H + \sum_{n=1, n \neq l}^L \sum_{m=1}^K \bar{\mathbf{H}}_{n,l,k} \mathbf{F}_{n,m} \mathbf{F}_{n,m}^H \bar{\mathbf{H}}_{n,l,k}^H + \sigma^2 \mathbf{I}. \quad (5)$$

B. Problem Formulation

In this paper, we aim to optimize the WSR of all the users through jointly optimizing the precoding matrices \mathbf{F} at the BSs and the phase shifts $\boldsymbol{\theta}$ at the IRS while guaranteeing the total power constraint at each BS. In specific, the WSR maximization problem is formulated as follows:

$$\max_{\mathbf{F}, \boldsymbol{\theta}} \sum_{l=1}^L \sum_{k=1}^K \omega_{l,k} R_{l,k}(\mathbf{F}, \boldsymbol{\theta}) \quad (6a)$$

$$\text{s.t.} \quad \sum_{k=1}^K \|\mathbf{F}_{l,k}\|_F^2 \leq P_{l,\max}, l = 1, \dots, L, \quad (6b)$$

$$0 \leq \theta_m \leq 2\pi, m = 1, \dots, M, \quad (6c)$$

where $\omega_{l,k}$ denotes the weight factor to represent the priority of the corresponding user. Due to the coupling effect between the precoding matrices \mathbf{F} and the phase shifts $\boldsymbol{\theta}$, this optimization problem is very difficult to solve. In addition, the phase shift constraints in (6c) make the optimization more difficult to solve. In the following, we provide a low-complexity algorithm to solve Problem (6).

III. LOW-COMPLEXITY ALGORITHM DEVELOPMENT

In this section, we first reformulate the original problem into a more tractable form. Then, the BCD method is proposed to solve the formulated problem.

A. Reformulation of the Original Problem

In the following, we exploit the relationship between the data rate and the mean-square error (MSE) for the optimal decoding matrix. To reduce the decoding complexity, we consider the linear decoding matrix so that the estimated signal vector for each user is given by

$$\hat{\mathbf{s}}_{l,k} = \mathbf{U}_{l,k}^H \mathbf{y}_{l,k}, \forall l, k, \quad (7)$$

where $\mathbf{U}_{l,k} \in \mathbb{C}^{N_r \times d}$ is the decoding matrix for the k th user in the l th cell. Then, the MSE matrix for each user is given by

$$\mathbf{E}_{l,k} = \mathbb{E}_{\mathbf{s}, \mathbf{n}} \left[(\hat{\mathbf{s}}_{l,k} - \mathbf{s}_{l,k}) (\hat{\mathbf{s}}_{l,k} - \mathbf{s}_{l,k})^H \right] \quad (8)$$

$$\begin{aligned} &= (\mathbf{U}_{l,k}^H \bar{\mathbf{H}}_{l,l,k} \mathbf{F}_{l,k} - \mathbf{I}) (\mathbf{U}_{l,k}^H \bar{\mathbf{H}}_{l,l,k} \mathbf{F}_{l,k} - \mathbf{I})^H + \sum_{m=1, m \neq k}^K \mathbf{U}_{l,k}^H \bar{\mathbf{H}}_{l,l,k} \mathbf{F}_{l,m} \mathbf{F}_{l,m}^H \bar{\mathbf{H}}_{l,l,k}^H \mathbf{U}_{l,k} \\ &\quad + \sum_{n=1, n \neq l}^L \sum_{m=1}^K \mathbf{U}_{l,k}^H \bar{\mathbf{H}}_{n,l,k} \mathbf{F}_{n,m} \mathbf{F}_{n,m}^H \bar{\mathbf{H}}_{n,l,k}^H \mathbf{U}_{l,k} + \sigma^2 \mathbf{U}_{l,k}^H \mathbf{U}_{l,k}, \forall l, k. \end{aligned} \quad (9)$$

By introducing a set of auxiliary matrices $\mathbf{W} = \{\mathbf{W}_{l,k} \succeq \mathbf{0}, \forall l, k\}$ and defining $\mathbf{U} = \{\mathbf{U}_{l,k}, \forall l, k\}$, Problem (6) can be reformulated as follows [27]:

$$\max_{\mathbf{W}, \mathbf{U}, \mathbf{F}, \boldsymbol{\theta}} \quad \sum_{l=1}^L \sum_{k=1}^K \omega_{l,k} h_{l,k}(\mathbf{W}, \mathbf{U}, \mathbf{F}, \boldsymbol{\theta}) \quad (10a)$$

$$\text{s.t.} \quad \sum_{k=1}^K \|\mathbf{F}_{l,k}\|_F^2 \leq P_{l,\max}, l = 1, \dots, L, \quad (10b)$$

$$0 \leq \theta_m \leq 2\pi, m = 1, \dots, M, \quad (10c)$$

where $h_{l,k}(\mathbf{W}, \mathbf{U}, \mathbf{F}, \boldsymbol{\theta})$ is given by

$$h_{l,k}(\mathbf{W}, \mathbf{U}, \mathbf{F}, \boldsymbol{\theta}) = \log |\mathbf{W}_{l,k}| - \text{Tr}(\mathbf{W}_{l,k} \mathbf{E}_{l,k}) + d. \quad (11)$$

Note that comparing with the original objective function in Problem (6), the new objective function in Problem (10) is in a more tractable form although we have introduced more optimization variables. For given phase shifts $\boldsymbol{\theta}$, $h_{l,k}(\mathbf{W}, \mathbf{U}, \mathbf{F}, \boldsymbol{\theta})$ is a concave function for each set of the optimization matrices when the other two are fixed. In the following, we propose the BCD algorithm to solve Problem (10). In specific, we maximize the objective function in (10) by alternatively optimizing one set of optimization variables while keeping the other variables fixed. Note that the decoding matrix $\mathbf{U}_{l,k}$ and the auxiliary matrix $\mathbf{W}_{l,k}$ are only related to $h_{l,k}(\mathbf{W}, \mathbf{U}, \mathbf{F}, \boldsymbol{\theta})$. In the following, we can derive the optimal solution for $\mathbf{U}_{l,k}$ and $\mathbf{W}_{l,k}$ when the other matrices are fixed.

For given $\boldsymbol{\theta}$, \mathbf{W} , and \mathbf{F} , by checking the first-order derivative of $h_{l,k}(\mathbf{W}, \mathbf{U}, \mathbf{F}, \boldsymbol{\theta})$ with respect to $\mathbf{U}_{l,k}$ and setting it to zero, we can obtain the optimal $\mathbf{U}_{l,k}$:

$$\mathbf{U}_{l,k} = (\mathbf{J}_{l,k} + \bar{\mathbf{H}}_{l,l,k} \mathbf{F}_{l,k} \mathbf{F}_{l,k}^H \bar{\mathbf{H}}_{l,l,k}^H)^{-1} \bar{\mathbf{H}}_{l,l,k} \mathbf{F}_{l,k}. \quad (12)$$

Similarly, for given $\boldsymbol{\theta}$, \mathbf{U} , and \mathbf{F} , the optimal auxiliary matrix $\mathbf{W}_{l,k}$ can be obtained as follows:

$$\mathbf{W}_{l,k} = \mathbf{E}_{l,k}^{-1}, \quad (13)$$

where $\mathbf{E}_{l,k}$ is given in (9).

In the following, we focus on optimizing the precoding matrices \mathbf{F} and phase shifts $\boldsymbol{\theta}$.

B. Optimizing Precoding Matrices \mathbf{F}

In this subsection, we focus on optimizing the precoding matrices \mathbf{F} while fixing \mathbf{W} , \mathbf{U} and $\boldsymbol{\theta}$. By substituting $\mathbf{E}_{l,k}$ into (11), the optimization over \mathbf{F} can be decoupled among different BSs. In specific, by removing the constant terms, the precoding matrices optimization problem for the l th BS is given by

$$\begin{aligned} \min_{\mathbf{F}_{l,k}, \forall k} \quad & \sum_{n=1}^L \sum_{m=1}^K \omega_{n,m} \text{Tr} \left(\mathbf{W}_{n,m} \sum_{k=1}^K \mathbf{U}_{n,m}^H \bar{\mathbf{H}}_{l,n,m} \mathbf{F}_{l,k} \mathbf{F}_{l,k}^H \bar{\mathbf{H}}_{l,n,m}^H \mathbf{U}_{n,m} \right) \\ & - \sum_{k=1}^K \omega_{l,k} \text{Tr} (\mathbf{W}_{l,k} \mathbf{U}_{l,k}^H \bar{\mathbf{H}}_{l,l,k} \mathbf{F}_{l,k}) - \sum_{k=1}^K \omega_{l,k} \text{Tr} (\mathbf{W}_{l,k} \mathbf{F}_{l,k}^H \bar{\mathbf{H}}_{l,l,k}^H \mathbf{U}_{l,k}) \end{aligned} \quad (14a)$$

$$\text{s.t.} \quad \sum_{k=1}^K \|\mathbf{F}_{l,k}\|_F^2 \leq P_{l,\max}. \quad (14b)$$

It can be readily verified that the above problem is a convex optimization problem, which can be transformed into a second order conic programming (SOCP) that can be efficiently solved by using the standard optimization packages such as CVX [28]. However, the computational complexity of solving an SOCP problem is very high. To reduce the complexity, in the following we provide a nearly optimal closed-form expression of the precoding matrices by using the Lagrangian multiplier method.

With some simple manipulations, the Lagrangian function of Problem (14) is written as

$$\begin{aligned} \mathcal{L}(\mathbf{F}_{l,k}, \forall k, \lambda_l) = & \sum_{k=1}^K \text{tr} (\mathbf{F}_{l,k}^H (\mathbf{A}_l + \lambda_l \mathbf{I}) \mathbf{F}_{l,k}) - \sum_{k=1}^K \omega_{l,k} \text{Tr} (\mathbf{W}_{l,k} \mathbf{U}_{l,k}^H \bar{\mathbf{H}}_{l,l,k} \mathbf{F}_{l,k}) \\ & - \sum_{k=1}^K \omega_{l,k} \text{Tr} (\mathbf{W}_{l,k} \mathbf{F}_{l,k}^H \bar{\mathbf{H}}_{l,l,k}^H \mathbf{U}_{l,k}) - \lambda_l P_{l,\max}, \end{aligned} \quad (15)$$

where $\lambda_l \geq 0$ is the Lagrangian multiplier associated with the power constraint for the l th BS, and $\mathbf{A}_{l,k}$ is given by

$$\mathbf{A}_l = \sum_{n=1}^L \sum_{m=1}^K \omega_{n,m} \bar{\mathbf{H}}_{l,n,m}^H \mathbf{U}_{n,m} \mathbf{W}_{n,m} \mathbf{U}_{n,m}^H \bar{\mathbf{H}}_{l,n,m}. \quad (16)$$

By setting the first-order derivative of $\mathcal{L}(\mathbf{F}_{l,k}, \forall k, \lambda_l)$ w.r.t. $\mathbf{F}_{l,k}$ to zero, we can obtain the optimal solution of $\mathbf{F}_{l,k}$ as follows:

$$\mathbf{F}_{l,k}(\lambda_l) = \omega_{l,k} (\mathbf{A}_l + \lambda_l \mathbf{I})^\dagger \bar{\mathbf{H}}_{l,l,k}^H \mathbf{U}_{l,k} \mathbf{W}_{l,k}, \quad (17)$$

where $(\cdot)^\dagger$ denotes the matrix pseudoinverse. The value of λ_l should be chosen such that the complementary slackness condition for the power constraint is satisfied:

$$\lambda_l \left(\sum_{k=1}^K \|\mathbf{F}_{l,k}(\lambda_l)\|_F^2 - P_{l,\max} \right) = 0. \quad (18)$$

In the following, we elaborate how to obtain the optimal λ_l , which is divided into two cases: 1) \mathbf{A}_l is full rank; 2) \mathbf{A}_l is low rank.

1) *Case I: \mathbf{A}_l is full rank:* In this case, \mathbf{A}_l is a positive definite matrix. It can be decomposed as $\mathbf{A}_l = \mathbf{Q}_l \mathbf{\Lambda}_l \mathbf{Q}_l^H$ by using the singular value decomposition (SVD), where $\mathbf{Q}_l \mathbf{Q}_l^H = \mathbf{Q}_l^H \mathbf{Q}_l = \mathbf{I}_{N_t}$ and $\mathbf{\Lambda}_l$ is a diagonal matrix with positive diagonal elements. Then, we have

$$\begin{aligned} f_l(\lambda_l) &\triangleq \sum_{k=1}^K \text{tr}(\mathbf{F}_{l,k}(\lambda_l)^H \mathbf{F}_{l,k}(\lambda_l)) \\ &= \sum_{k=1}^L \omega_{l,k}^2 \text{tr}(\mathbf{W}_{l,k}^H \mathbf{U}_{l,k}^H \bar{\mathbf{H}}_{l,l,k} (\mathbf{A}_l + \lambda_l \mathbf{I})^{-1} (\mathbf{A}_l + \lambda_l \mathbf{I})^{-1} \bar{\mathbf{H}}_{l,l,k}^H \mathbf{U}_{l,k} \mathbf{W}_{l,k}) \end{aligned} \quad (19)$$

$$= \sum_{k=1}^L \omega_{l,k}^2 \text{tr}(\mathbf{W}_{l,k}^H \mathbf{U}_{l,k}^H \bar{\mathbf{H}}_{l,l,k} (\mathbf{Q}_l \mathbf{\Lambda}_l \mathbf{Q}_l^H + \lambda_l \mathbf{I})^{-1} (\mathbf{Q}_l \mathbf{\Lambda}_l \mathbf{Q}_l^H + \lambda_l \mathbf{I})^{-1} \bar{\mathbf{H}}_{l,l,k}^H \mathbf{U}_{l,k} \mathbf{W}_{l,k}) \quad (20)$$

$$= \sum_{k=1}^L \omega_{l,k}^2 \text{tr}(\mathbf{W}_{l,k}^H \mathbf{U}_{l,k}^H \bar{\mathbf{H}}_{l,l,k} \mathbf{Q}_l (\mathbf{\Lambda}_l + \lambda_l \mathbf{I})^{-2} \mathbf{Q}_l^H \bar{\mathbf{H}}_{l,l,k}^H \mathbf{U}_{l,k} \mathbf{W}_{l,k}) \quad (21)$$

$$= \text{tr}((\mathbf{\Lambda}_l + \lambda_l \mathbf{I})^{-2} \mathbf{Z}_l) \quad (22)$$

$$= \sum_{i=1}^{N_t} \frac{[\mathbf{Z}_l]_{i,i}}{([\mathbf{\Lambda}_l]_{i,i} + \lambda_l)^2} \quad (23)$$

where $\mathbf{Z}_l = \sum_{k=1}^L \omega_{l,k}^2 \mathbf{Q}_l^H \bar{\mathbf{H}}_{l,l,k}^H \mathbf{U}_{l,k} \mathbf{W}_{l,k} \mathbf{W}_{l,k}^H \mathbf{U}_{l,k}^H \bar{\mathbf{H}}_{l,l,k} \mathbf{Q}_l$, $[\mathbf{Z}_l]_{i,i}$ and $[\mathbf{\Lambda}_l]_{i,i}$ denote the i th diagonal element of matrix \mathbf{Z}_l and matrix $\mathbf{\Lambda}_l$, respectively. It can be readily verified that $f_l(\lambda_l)$ is a monotonically decreasing function. Hence, if $f_l(0) \leq P_{l,\max}$, then the optimal precoding matrix is

given by $\mathbf{F}_{l,k}^{\text{opt}} = \mathbf{F}_{l,k}(0)$, otherwise, the optimal λ_l can be obtained by using the bisection search method to find the solution to the following equation:

$$f_l(\lambda_l) = \sum_{i=1}^{N_t} \frac{[\mathbf{Z}_l]_{i,i}}{([\mathbf{\Lambda}_l]_{i,i} + \lambda_l)^2} = P_{l,\max}. \quad (24)$$

Since $f_l(\infty) = 0$, the solution to Equation (24) must exist, which is denoted as λ_l^{opt} . Then, the optimal precoding matrix can be obtained as $\mathbf{F}_{l,k}^{\text{opt}} = \mathbf{F}_{l,k}(\lambda_l^{\text{opt}})$. To apply the bisection search method, we need to find the upper bound of λ_l , which is given by

$$\lambda_l < \sqrt{\frac{\sum_{i=1}^{N_t} [\mathbf{Z}_l]_{i,i}}{P_{l,\max}}} \triangleq \lambda_l^{\text{ub}}. \quad (25)$$

This can be proved as follows:

$$f_l(\lambda_l^{\text{ub}}) = \sum_{i=1}^{N_t} \frac{[\mathbf{Z}_l]_{i,i}}{([\mathbf{\Lambda}_l]_{i,i} + \lambda_l^{\text{ub}})^2} < \sum_{i=1}^{N_t} \frac{[\mathbf{Z}_l]_{i,i}}{(\lambda_l^{\text{ub}})^2} = P_{l,\max}. \quad (26)$$

2) *Case II: \mathbf{A}_l is low rank:* In this case, the above method cannot be directly applied since the \mathbf{Q}_l obtained by SVD is not a unitary matrix and derivation in (21) cannot be obtained. To resolve this issue, we first check whether $\lambda_l = 0$ is the optimal solution or not. If

$$f_l(0) = \sum_{k=1}^K \text{tr}(\mathbf{F}_{l,k}(0)^H \mathbf{F}_{l,k}(0)) \leq P_{l,\max}, \quad (27)$$

then the optimal precoding matrix is given by $\mathbf{F}_{l,k}^{\text{opt}} = \mathbf{F}_{l,k}(0)$, otherwise, the optimal λ_l is a positive value, which will be obtained as follows. Define the rank of \mathbf{A}_l as $r_l = \text{rank}(\mathbf{A}_l) < N_t$ and using the SVD, we have

$$\mathbf{A}_l = [\mathbf{Q}_{l,1}, \mathbf{Q}_{l,2}] \mathbf{\Lambda}_l [\mathbf{Q}_{l,1}, \mathbf{Q}_{l,2}]^H, \quad (28)$$

where $\mathbf{Q}_{l,1}$ contains the first r_l singular vectors corresponding to the r_l positive eigenvalues, and $\mathbf{Q}_{l,2}$ holds the last $N_t - r_l$ singular vectors corresponding to the $N_t - r_l$ zero-valued eigenvalues, $\mathbf{\Lambda}_l = \text{diag}\{\mathbf{\Lambda}_{l,1}, \mathbf{0}_{(N_t-r_l) \times (N_t-r_l)}\}$ with $\mathbf{\Lambda}_{l,1}$ denoting the diagonal matrix containing the first r_l positive eigenvalues. Define $\mathbf{Q}_l \triangleq [\mathbf{Q}_{l,1}, \mathbf{Q}_{l,2}]$ and apply the similar derivations from (19) to (23), we have

$$f_l(\lambda_l) = \sum_{k=1}^K \text{tr}(\mathbf{F}_{l,k}(\lambda_l)^H \mathbf{F}_{l,k}(\lambda_l)) \quad (29)$$

$$= \sum_{i=1}^{r_l} \frac{[\mathbf{Z}_l]_{i,i}}{([\mathbf{\Lambda}_l]_{i,i} + \lambda_l)^2} + \sum_{i=r_l+1}^{N_t} \frac{[\mathbf{Z}_l]_{i,i}}{\lambda_l^2}, \quad (30)$$

where \mathbf{Z}_l is the same as that in Case I. Obviously, $f_l(\lambda_l)$ is a monotonically decreasing function for $\lambda_l > 0$ and the optimal λ_l can be obtained by using the bisection search method where the lower bound of λ_l is set as a very small positive value.

C. Optimizing Phase Shifts θ

In this subsection, we focus on optimizing the phase shifts θ while fixing \mathbf{W} , \mathbf{U} and \mathbf{F} . By substituting $\mathbf{E}_{l,k}$ into (11) and ignoring the terms that are not related to the channels, the phase shift optimization problem is given by

$$\begin{aligned} \min_{\theta} \quad & \sum_{l=1}^L \sum_{n=1}^L \sum_{m=1}^K \text{Tr} \left(\omega_{n,m} \mathbf{W}_{n,m} \mathbf{U}_{n,m}^H \bar{\mathbf{H}}_{l,n,m} \mathbf{F}_l \bar{\mathbf{H}}_{l,n,m}^H \mathbf{U}_{n,m} \right) \\ & - \sum_{l=1}^L \sum_{k=1}^K \text{Tr} \left(\omega_{l,k} \mathbf{W}_{l,k} \mathbf{U}_{l,k}^H \bar{\mathbf{H}}_{l,l,k} \mathbf{F}_{l,k} \right) - \sum_{l=1}^L \sum_{k=1}^K \text{Tr} \left(\omega_{l,k} \mathbf{W}_{l,k} \mathbf{F}_{l,k}^H \bar{\mathbf{H}}_{l,l,k}^H \mathbf{U}_{l,k} \right) \end{aligned} \quad (31a)$$

$$\text{s.t.} \quad 0 \leq \theta_m \leq 2\pi, m = 1, \dots, M, \quad (31b)$$

where $\mathbf{F}_l = \sum_{k=1}^K \mathbf{F}_{l,k} \mathbf{F}_{l,k}^H$.

By using $\bar{\mathbf{H}}_{l,n,m} = \mathbf{H}_{r,n,m} \Phi \mathbf{G}_{l,r} + \mathbf{H}_{l,n,m}$, we have

$$\begin{aligned} & \omega_{n,m} \mathbf{W}_{n,m} \mathbf{U}_{n,m}^H \bar{\mathbf{H}}_{l,n,m} \mathbf{F}_l \bar{\mathbf{H}}_{l,n,m}^H \mathbf{U}_{n,m} \\ &= \omega_{n,m} \mathbf{W}_{n,m} \mathbf{U}_{n,m}^H \mathbf{H}_{r,n,m} \Phi \mathbf{G}_{l,r} \mathbf{F}_l \mathbf{G}_{l,r}^H \Phi^H \mathbf{H}_{r,n,m}^H \mathbf{U}_{n,m} + \omega_{n,m} \mathbf{W}_{n,m} \mathbf{U}_{n,m}^H \mathbf{H}_{l,n,m} \mathbf{F}_l \mathbf{G}_{l,r}^H \Phi^H \mathbf{H}_{r,n,m}^H \mathbf{U}_{n,m} \\ & \quad + \omega_{n,m} \mathbf{W}_{n,m} \mathbf{U}_{n,m}^H \mathbf{H}_{r,n,m} \Phi \mathbf{G}_{l,r} \mathbf{F}_l \mathbf{H}_{l,n,m}^H \mathbf{U}_{n,m} + \omega_{n,m} \mathbf{W}_{n,m} \mathbf{U}_{n,m}^H \mathbf{H}_{l,n,m} \mathbf{F}_l \mathbf{H}_{l,n,m}^H \mathbf{U}_{n,m} \end{aligned} \quad (32)$$

and

$$\omega_{l,k} \mathbf{W}_{l,k} \mathbf{U}_{l,k}^H \bar{\mathbf{H}}_{l,l,k} \mathbf{F}_{l,k} = \omega_{l,k} \mathbf{W}_{l,k} \mathbf{U}_{l,k}^H \mathbf{H}_{r,l,k} \Phi \mathbf{G}_{l,r} \mathbf{F}_{l,k} + \omega_{l,k} \mathbf{W}_{l,k} \mathbf{U}_{l,k}^H \mathbf{H}_{l,l,k} \mathbf{F}_{l,k}. \quad (33)$$

By defining $\mathbf{B}_{n,m} \triangleq \omega_{n,m} \mathbf{H}_{r,n,m}^H \mathbf{U}_{n,m} \mathbf{W}_{n,m} \mathbf{U}_{n,m}^H \mathbf{H}_{r,n,m}$, $\mathbf{C}_l \triangleq \mathbf{G}_{l,r} \mathbf{F}_l \mathbf{G}_{l,r}^H$ and

$$\mathbf{D}_{l,n,m} \triangleq \omega_{n,m} \mathbf{G}_{l,r} \mathbf{F}_l^H \mathbf{H}_{l,n,m}^H \mathbf{U}_{n,m} \mathbf{W}_{n,m} \mathbf{U}_{n,m}^H \mathbf{H}_{r,n,m},$$

from (32) we have

$$\begin{aligned} & \text{Tr} \left(\omega_{n,m} \mathbf{W}_{n,m} \mathbf{U}_{n,m}^H \bar{\mathbf{H}}_{l,n,m} \mathbf{F}_l \bar{\mathbf{H}}_{l,n,m}^H \mathbf{U}_{n,m} \right) \\ &= \text{Tr} \left(\Phi^H \mathbf{B}_{n,m} \Phi \mathbf{C}_l \right) + \text{Tr} \left(\Phi^H \mathbf{D}_{l,n,m}^H \right) + \text{Tr} \left(\Phi \mathbf{D}_{l,n,m} \right) + \text{const}_1 \end{aligned} \quad (34)$$

where const_1 is a constant term that does not depend on Φ .

Similarly, by defining $\mathbf{T}_{l,k} \triangleq \omega_{l,k} \mathbf{G}_{l,r} \mathbf{F}_{l,k} \mathbf{W}_{l,k} \mathbf{U}_{l,k}^H \mathbf{H}_{r,l,k}$, from (33) we have

$$\text{Tr} \left(\omega_{l,k} \mathbf{W}_{l,k} \mathbf{U}_{l,k}^H \bar{\mathbf{H}}_{l,l,k} \mathbf{F}_{l,k} \right) = \text{Tr} \left(\Phi \mathbf{T}_{l,k} \right) + \text{const}_2 \quad (35)$$

where const_2 is a constant term that is independent of Φ .

By substituting (34) and (35) into the objective function of Problem (31) and ignoring the constant terms, we have

$$\min_{\boldsymbol{\theta}} \quad \text{Tr}(\boldsymbol{\Phi}^H \mathbf{B} \boldsymbol{\Phi} \mathbf{C}) + \text{Tr}(\boldsymbol{\Phi}^H \mathbf{V}^H) + \text{Tr}(\boldsymbol{\Phi} \mathbf{V}) \quad (36a)$$

$$\text{s.t.} \quad 0 \leq \theta_m \leq 2\pi, m = 1, \dots, M, \quad (36b)$$

where \mathbf{B} , \mathbf{C} and \mathbf{V} are respectively given by

$$\mathbf{B} = \sum_{n=1}^L \sum_{m=1}^K \mathbf{B}_{n,m}, \mathbf{C} = \sum_{l=1}^L \mathbf{C}_l, \mathbf{V} = \sum_{l=1}^L \sum_{n=1}^L \sum_{m=1}^K \mathbf{D}_{l,n,m} - \sum_{l=1}^L \sum_{k=1}^K \mathbf{T}_{l,k}. \quad (37)$$

Denote $\boldsymbol{\phi} \triangleq [e^{j\theta_1}, \dots, e^{j\theta_m}, \dots, e^{j\theta_M}]^T$, which is the collection of diagonal elements of $\boldsymbol{\Phi}$. By using the matrix identity in [29, Eq. (1.10.6)], we have

$$\text{Tr}(\boldsymbol{\Phi}^H \mathbf{B} \boldsymbol{\Phi} \mathbf{C}) = \boldsymbol{\phi}^H (\mathbf{B} \odot \mathbf{C}^T) \boldsymbol{\phi}. \quad (38)$$

Let \mathbf{v} be the collection of diagonal elements of matrix \mathbf{V} , given by $\mathbf{v} = [\mathbf{V}_{1,1}, \dots, \mathbf{V}_{M,M}]^T$.

Then, we have

$$\text{Tr}(\boldsymbol{\Phi} \mathbf{V}) = \boldsymbol{\phi}^T \mathbf{v}, \text{Tr}(\boldsymbol{\Phi}^H \mathbf{V}^H) = \mathbf{v}^H \boldsymbol{\phi}^*. \quad (39)$$

Hence, Problem (36) can be rewritten as

$$\min_{\boldsymbol{\theta}} \quad \boldsymbol{\phi}^H \boldsymbol{\Xi} \boldsymbol{\phi} + \boldsymbol{\phi}^T \mathbf{v} + \mathbf{v}^H \boldsymbol{\phi}^* \quad (40a)$$

$$\text{s.t.} \quad 0 \leq \theta_m \leq 2\pi, m = 1, \dots, M, \quad (40b)$$

where $\boldsymbol{\Xi} = \mathbf{B} \odot \mathbf{C}^T$. It can be readily verified that \mathbf{B} and \mathbf{C}^T are semidefinite matrices. Then, according to Property (9) on Page 104 of [29], the Hadamard product $\mathbf{B} \odot \mathbf{C}^T$ (or equivalently $\boldsymbol{\Xi}$) is also a semidefinite matrix.

Let $\phi_m = e^{j\theta_m}, \forall m$, and then $\boldsymbol{\phi} = [\phi_1, \dots, \phi_M]^T$. Problem (40) can be equivalently rewritten as

$$\min_{\boldsymbol{\phi}} \quad f(\boldsymbol{\phi}) \triangleq \boldsymbol{\phi}^H \boldsymbol{\Xi} \boldsymbol{\phi} + 2\text{Re}\{\boldsymbol{\phi}^H \mathbf{v}^*\} \quad (41a)$$

$$\text{s.t.} \quad |\phi_m| = 1, m = 1, \dots, M. \quad (41b)$$

Due to the unit modulus constraint in (41b), Problem (41) is a non-convex optimization problem. In the following, we provide two efficient algorithms to solve this problem.

1) *Majorization-Minimization (MM) Algorithm:* We adopt the MM algorithm [30] to solve Problem (41). The main idea is to deal with a difficult problem by constructing a series of more tractable approximate subproblems. In specific, denote ϕ^t as the solution of the subproblem in the t th iteration, and $f(\phi^t)$ is the objective value of Problem (41) in the t th iteration. In the $(t+1)$ th iteration, we need to introduce an upper bound² on the objective function based on the previous solution, which is denoted as $g(\phi|\phi^t)$. We solve the approximate subproblem with new objective function $g(\phi|\phi^t)$ in the $(t+1)$ th iteration. If function $g(\phi|\phi^t)$ satisfies the following three conditions:

- 1) $g(\phi^t|\phi^t) = f(\phi^t)$,
- 2) $\nabla_{\phi} g(\phi|\phi^t)|_{\phi=\phi^t} = \nabla_{\phi} f(\phi^t)|_{\phi=\phi^t}$,
- 3) $g(\phi|\phi^t) \geq f(\phi)$,

then the sequence of the solutions obtained in each iteration will incur a monotonically decreasing objective function $\{f(\phi^t), t = 1, 2, \dots\}$ and finally converge. The converged solution satisfies the Karush-Kuhn-Tucker (KKT) optimality conditions of Problem (41) [31]. The first two conditions mean that the introduced function $g(\phi|\phi^t)$ and its first-order gradient should be the same as the original function and its first-order gradient at point ϕ^t . The third condition means that the constructed function $g(\phi|\phi^t)$ should be the upper bound of the original objective function. To make this algorithm work, the most important task is to find $g(\phi|\phi^t)$, which should satisfy these three conditions and should be much more tractable than $f(\phi)$.

To this end, we first introduce the following lemma proposed in [32].

Lemma 1: For any given solution ϕ^t at the t th iteration and for any feasible ϕ , we have

$$\phi^H \Xi \phi \leq \phi^H \mathbf{X} \phi - 2\text{Re} \{ \phi^H (\mathbf{X} - \Xi) \phi^t \} + (\phi^t)^H (\mathbf{X} - \Xi) \phi^t \triangleq y(\phi|\phi^t), \quad (42)$$

where $\mathbf{X} = \lambda_{\max} \mathbf{I}_M$ and λ_{\max} is the maximum eigenvalue of Ξ . □

By constructing the surrogate function $g(\phi|\phi^t)$ as follows:

$$g(\phi|\phi^t) = y(\phi|\phi^t) + 2\text{Re} \{ \phi^H \mathbf{v}^* \}, \quad (43)$$

where $y(\phi|\phi^t)$ is defined in (42). It can be readily verified that $g(\phi|\phi^t)$ given in (43) satisfies the three conditions. In addition, $g(\phi|\phi^t)$ is more tractable to handle than the original objective

²Please note that we consider the minimization problem here.

function $f(\phi)$. In specific, the subproblem to be solved in the t th iteration is given by

$$\min_{\phi} \quad g(\phi|\phi^t) \quad (44a)$$

$$\text{s.t.} \quad |\phi_m| = 1, m = 1, \dots, M. \quad (44b)$$

Since $\phi^H \phi = M$, we have $\phi^H \mathbf{X} \phi = M \lambda_{\max}$, which is a constant. By removing the other constants, Problem (44) can be rewritten as follows:

$$\max_{\phi} \quad 2\text{Re} \left\{ \phi^H \mathbf{q}^t \right\} \quad (45a)$$

$$\text{s.t.} \quad |\phi_m| = 1, m = 1, \dots, M, \quad (45b)$$

where $\mathbf{q}^t = (\lambda_{\max} \mathbf{I}_M - \Xi) \phi^t - \mathbf{v}^*$. The optimal solution of Problem (45) is given by

$$\phi^{t+1} = e^{j \arg(\mathbf{q}^t)}. \quad (46)$$

Based on the above discussion, we provide the details of the MM algorithm in Algorithm 1. When the algorithm converges, we can obtain the optimal phase shift as $\theta^* = \arg(\mathbf{q}^t)$.

Algorithm 1 MM Algorithm

- 1: Initial the iteration number $t = 1$, the accuracy ε . Input the feasible solution ϕ^0 . Calculate the value of the objective function in Problem (41) as $f(\phi^1)$;
 - 2: Calculate $\mathbf{q}^t = (\lambda_{\max} \mathbf{I}_M - \Xi) \phi^t - \mathbf{v}^*$;
 - 3: Update ϕ^{t+1} in (46);
 - 4: Calculate the objective function $f(\phi^{t+1})$, if $|f(\phi^{t+1}) - f(\phi^t)|/f(\phi^{t+1}) \leq \varepsilon$ holds, terminate; Otherwise, set $t \leftarrow t + 1$ and go to step 2.
-

2) *Complex Circle Manifold (CCM) Method:* In this subsection, we adopt the CCM method proposed in recent work [33] to directly solve Problem (41). We first transform Problem (41) into the following equivalent problem as

$$\min_{\phi} \quad \bar{f}(\phi) \triangleq \phi^H (\Xi + \alpha \mathbf{I}_M) \phi + 2\text{Re} \{ \phi^H \mathbf{v}^* \} \quad (47a)$$

$$\text{s.t.} \quad |\phi_m| = 1, m = 1, \dots, M. \quad (47b)$$

where $\alpha > 0$ is a positive constant parameter, the value of which will be given later. Problem (41) is equivalent to Problem (47) since $\alpha \phi^H \phi = \alpha M$. The parameter α can control the convergence of the CCM method, which will be discussed later.

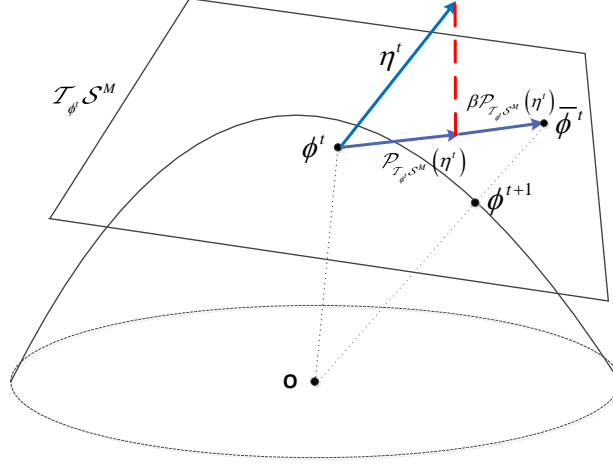


Fig. 2. Geometric interpretation of the CCM algorithm.

The search space in Problem (47) can be regarded as the product of M complex circles³, which is a sub-manifold of \mathbb{C}^M given by

$$\mathcal{S}^M \triangleq \{\mathbf{x} \in \mathbb{C}^M : |x_l| = 1, l = 1, 2, \dots, M\}, \quad (48)$$

where x_l is the l th element of vector \mathbf{x} .

The main idea of CCM algorithm is to derive a gradient descent algorithm based on the manifold space defined in (48), which is similar to the concept of the gradient descent developed for the conventional optimization over the Euclidean space. The main steps of the CCM algorithm is composed of four main steps in each iteration t :

1) *Gradient in Euclidean Space*: We first need to find the search direction and the most common search direction for the minimization problem is the negative gradient of $\bar{f}(\phi^t)$, which is given by

$$\boldsymbol{\eta}^t = -\nabla_{\phi} \bar{f}(\phi^t) = -2(\boldsymbol{\Xi} + \alpha \mathbf{I}_M) \phi^t - 2\mathbf{v}^*. \quad (49)$$

2) *Riemannian gradients*: Since we optimize over the manifold space, we need to find the Riemannian gradient [9]. The Riemannian gradient of $\bar{f}(\phi^t)$ at the current point $\phi^t \in \mathcal{S}^M$ is in the tangent space $\mathcal{T}_{\phi^t} \mathcal{S}^M$ ⁴. In specific, the Riemannian gradient of $\bar{f}(\phi^t)$ at ϕ^t can be obtained by

³Each complex circle is given by $\mathcal{S} \triangleq \{x \in \mathbb{C} : x^* x = \text{Re}\{x\}^2 + \text{Im}\{x\}^2 = 1\}$, which is a sub-manifold of \mathbb{C} [33].

⁴The tangent space of \mathcal{S} at point z_m is defined as $\mathcal{T}_{z_m} \mathcal{S} = \{x \in \mathbb{C} : \text{Re}\{x^* z_m\} = 0\}$. Then, the tangent space $\mathcal{T}_{\mathbf{z}} \mathcal{S}^M$ is the product of these M tangent space $\mathcal{T}_{z_m} \mathcal{S}$ given by $\mathcal{T}_{\mathbf{z}} \mathcal{S}^M = \mathcal{T}_{z_1} \mathcal{S} \times \mathcal{T}_{z_2} \mathcal{S} \cdots \times \mathcal{T}_{z_M} \mathcal{S}$.

projecting the search direction $\boldsymbol{\eta}^t$ in Euclidean space onto $\mathcal{T}_{\phi^t}\mathcal{S}^M$ by using the projection operator, which can be calculated as follows [9]:

$$\mathbf{P}_{\mathcal{T}_{\phi^t}\mathcal{S}^M}(\boldsymbol{\eta}^t) = \boldsymbol{\eta}^t - \text{Re}\{\boldsymbol{\eta}^{t*} \odot \phi^t\} \odot \phi^t. \quad (50)$$

3) *Update over the tangent space*: Update the current point ϕ^t on the tangent space $\mathcal{T}_{\phi^t}\mathcal{S}^M$:

$$\bar{\phi}^t = \phi^t + \beta \mathbf{P}_{\mathcal{T}_{\phi^t}\mathcal{S}^M}(\boldsymbol{\eta}^t), \quad (51)$$

where β is a constant step size that will be discussed later.

4) *Retraction operator*: In general, the obtained $\bar{\phi}^t$ is not in \mathcal{S}^M , i.e., $\bar{\phi}^t \notin \mathcal{S}^M$. It needs to be mapped into the manifold \mathcal{S}^M by using the retraction operator⁵ as follows

$$\phi^{t+1} = \bar{\phi}^t \odot \frac{1}{|\bar{\phi}^t|}. \quad (52)$$

Note that both ϕ^{t+1} and ϕ^t belongs to \mathcal{S}^M , which satisfies the unit constant modulus constraints. The details of the CCM algorithm is presented in Algorithm 2. The CCM algorithm is also geometrically illustrated in Fig. 2.

Algorithm 2 CCM Algorithm

- 1: Initial the iteration number $t = 1$, the accuracy ε . Input the feasible solution ϕ^1 . Calculate the value of the objective function in Problem (47) as $\bar{f}(\phi^1)$;
 - 2: Calculate the Euclidean gradient $\boldsymbol{\eta}^t$ in (49);
 - 3: Calculate the Riemannian gradient $\mathbf{P}_{\mathcal{T}_{\phi^t}\mathcal{S}^M}(\boldsymbol{\eta}^t)$ in (50);
 - 4: Update over the tangent space according to (51);
 - 5: Update ϕ^{t+1} by retracting $\bar{\phi}^t$ to the complex circle manifold \mathcal{S}^M according to (52);
 - 6: Calculate the objective function $\bar{f}(\phi^{t+1})$, if $|\bar{f}(\phi^{t+1}) - \bar{f}(\phi^t)| / \bar{f}(\phi^{t+1}) \leq \varepsilon$ holds, terminate; Otherwise, set $t \leftarrow t + 1$ and go to step 2.
-

The following theorem provides the guidance for the choices of parameters α and β to guarantee the convergence of the CCM algorithm.

Theorem 1 [33]: Let λ_{Ξ} and $\lambda_{\Xi+\alpha\mathbf{I}_M}$ be the largest eigenvalue of matrices Ξ and $\Xi + \alpha\mathbf{I}_M$, respectively. If α and β are chosen to satisfy the following conditions,

$$\alpha \geq \frac{M}{8} \lambda_{\Xi} + \|\mathbf{v}\|_2, 0 < \beta < \frac{1}{\lambda_{\Xi+\alpha\mathbf{I}}}, \quad (53)$$

⁵The retraction operator normalizes each element of $\bar{\phi}^t$ to be unit.

TABLE I
COMPUTATIONAL COMPLEXITY COMPARISON FOR TWO DIFFERENT ALGORITHMS TO FIND THE PHASE SHIFTS

Algorithms	MM Alg.	CCM Alg.
Complexity	$\mathcal{O}(M^3 + T_{MM}M^2)$	$\mathcal{O}(M^3 + T_{CCM}M^2)$

then the CCM algorithm generates a non-increasing sequence $\{\bar{f}(\phi^t), t = 1, 2, \dots\}$, and finally converges to a finite value. \square

3) *Complexity Analysis:* In this part, we analyze the complexity of the proposed two methods to solve Problem (41).

We now analyze the complexity of MM algorithm. At the beginning of the MM algorithm, one needs to calculate λ_{\max} , i.e., the maximum eigenvalue of Ξ . The complexity is given by $\mathcal{O}(M^3)$. For each iteration of the MM algorithm, the main complexity lies in the calculation of \mathbf{q}^t in step 2, the complexity of which is $\mathcal{O}(M^2)$. Denote T_{MM} as the number of iterations required for the MM algorithm to converge. Then, the total complexity of the MM algorithm is given by $C_{MM} = \mathcal{O}(M^3 + T_{MM}M^2)$.

We then analyze the complexity of the CCM algorithm. At the start of the CCM algorithm, we need to find the range of α and β to guarantee the convergence of the CCM algorithm, which needs to calculate the largest eigenvalue of matrices Ξ (λ_{Ξ}) as shown in Theorem 1. Its complexity is given by $\mathcal{O}(M^3)$. For each iteration of the CCM algorithm, the complexity mainly depends on the calculation of Euclidean gradient $\boldsymbol{\eta}^t$, which is given by $\mathcal{O}(M^2)$. Denote T_{CCM} as the total number of iterations for the CCM algorithm to converge. The total complexity of the CCM algorithm is given by $C_{CCM} = \mathcal{O}(M^3 + T_{CCM}M^2)$.

The computational complexity for these algorithms are summarized in Table I. It can be observed that which algorithm has lower complexity mainly depends on the number of iterations to converge. The simulation results will compare their convergence speed.

D. Overall Algorithm to Solve Problem (6)

Based on the above analysis, we provide the detailed description of the BCD algorithm to solve Problem (6) in Algorithm 3. In step 5, we need to apply three algorithms to solve Problem (41) to find the phase shifts $\boldsymbol{\theta}^{(n+1)}$. Both the MM algorithm and the CCM algorithm can guarantee to yield a decreasing objective value of Problem (41) compared with the previous phase solution,

i.e., $f(\phi^{(n+1)}) < f(\phi^{(n)})$. It can be readily verified that the objective value of Problem (10) monotonically increases in each step of Algorithm 3. In addition, due to the power constraints, the objective value has a upper bound. Hence, Algorithm 3 is guaranteed to converge.

Algorithm 3 Block Coordinate Descent Algorithm

- 1: Initialize iterative number $n = 1$, maximum number of iterations n_{\max} , feasible $\mathbf{F}^{(1)}$, $\boldsymbol{\theta}^{(0)}$, error tolerance ε , calculate the objective value of Problem (6), denoted as $\text{Obj}(\mathbf{F}^{(1)}, \boldsymbol{\theta}^{(1)})$;
 - 2: Given $\mathbf{F}^{(n)}$ and $\boldsymbol{\theta}^{(n)}$, calculate the optimal decoding matrices $\mathbf{U}^{(n)}$ in (12);
 - 3: Given $\mathbf{F}^{(n)}$, $\mathbf{U}^{(n)}$ and $\boldsymbol{\theta}^{(n)}$, calculate the optimal auxiliary matrices $\mathbf{W}^{(n)}$;
 - 4: Given $\mathbf{U}^{(n)}$, $\mathbf{W}^{(n)}$ and $\boldsymbol{\theta}^{(n)}$, calculate the optimal precoding matrices $\mathbf{F}^{(n+1)}$ by solving Problem (14) with the Lagrangian multiplier method in Subsection III-B;
 - 5: Given $\mathbf{U}^{(n)}$, $\mathbf{W}^{(n)}$ and $\mathbf{F}^{(n+1)}$, calculate the optimal $\boldsymbol{\theta}^{(n+1)}$ by solving Problem (41) with the algorithms developed in Subsection III-C;
 - 6: If $n \geq n_{\max}$ or $|\text{Obj}(\mathbf{F}^{(n+1)}, \boldsymbol{\theta}^{(n+1)}) - \text{Obj}(\mathbf{F}^{(n)}, \boldsymbol{\theta}^{(n)})| / \text{Obj}(\mathbf{F}^{(n+1)}, \boldsymbol{\theta}^{(n+1)}) < \varepsilon$, terminate. Otherwise, set $n \leftarrow n + 1$ and go to step 2.
-

Now, we analyze the computational complexity of the BCD algorithm. In step 2, the complexity of computing decoding matrices $\mathbf{U}^{(n)}$ is $\mathcal{O}(LKN_r^3)$. In step 3, the complexity of calculating the auxiliary matrices $\mathbf{W}^{(n)}$ is given by $\mathcal{O}(LKd^3)$. In step 4, we need to calculate the precoding matrices $\mathbf{F}^{(n+1)}$. The detailed analysis is provided as follows. For any two complex matrices $\mathbf{X} \in \mathbb{C}^{m \times n}$, $\mathbf{Y} \in \mathbb{C}^{n \times p}$, the complexity of computing \mathbf{XY} is $\mathcal{O}(mnp)$ [34]. We assume that $N_t > N_r > d$. Hence, the complexity of computing matrices $\{\mathbf{A}_{l,k}, \forall l, k\}$ in (16) is given by $\mathcal{O}(LKN_t^2d)$. The complexity of calculating $\mathbf{F}_{l,k}$ in (17) is given by $\mathcal{O}(LKN_t^3)$. The SVD decomposition of $\{\mathbf{A}_l, \forall l\}$ is given by $\mathcal{O}(LN_t^3)$. The complexity of calculating $\{\mathbf{Z}_l\}$ is given by $\mathcal{O}(L^2N_t^2N_r)$. The complexity of calculation the Lagrangian multipliers $\{\lambda_l, \forall l\}$ can be ignored. Hence, the overall complexity of calculating the precoding matrices $\mathbf{F}^{(n+1)}$ is given by $\mathcal{O}(\max\{LKN_t^3, L^2N_t^2N_r\})$. The complexity of calculating the optimal $\boldsymbol{\theta}^{(n+1)}$ is given in Table I, and the complexity for each algorithm is written as $C_i, i = \text{MM}, \text{CCM}$. Then, the overall complexity of the BCD algorithm is given by

$$C_{\text{BCD},i} = \mathcal{O}(\max\{LKN_t^3, L^2N_t^2N_r, C_i\}), i = \text{MM}, \text{CCM}, \quad (54)$$

where $C_{\text{BCD},i}$ denotes the overall complexity of the BCD algorithm when the phase shifts are obtained by using method i , $i = \text{MM}, \text{CCM}$.

IV. SIMULATION RESULTS

In this section, simulation results are provided to validate the benefits of deploying IRS to improve WSR performance of the multicell system. We consider a two-cell IRS-aided communication network shown in Fig. 3, in which there are two BSs located at $(0, 0)$ and $(600, 0)$, respectively. The location of the boundary point between two cells is $(300, 0)$. Two users in the first cell are uniformly and randomly placed in a circle centered at $(x_u, 0)$ with radius 20 m, while two users in the second cell are also uniformly and randomly distributed in a circle centered at $(600 - x_u, 0)$ with radius 20 m. Note that these two circles are symmetry at the boundary point. The IRS is located at $(x_{\text{IRS}}, 30)$, which means it lies in a horizontal line that is parallel to the one between two BSs and the vertical distance between two lines is 30 m. The large-scale path loss in dB is given by

$$\text{PL} = \text{PL}_0 - 10\alpha \log_{10} \left(\frac{d}{d_0} \right), \quad (55)$$

where PL_0 is the pass loss at reference distance d_0 , d is the link distance, α is the path loss exponent. In our simulation, we set $\text{PL}_0 = -30$ dB and $d_0 = 1$ m. Due to extensive obstacles and scatters, the path loss exponent between the BS and the users is given by $\alpha_{\text{BU}} = 3.75$. By carefully choosing the location of the IRS, the IRS-aided link has higher probability to experience nearly free-space path loss. Then, we set the path loss exponents of the BS-IRS link and the IRS-user link as $\alpha_{\text{BI}} = \alpha_{\text{IU}} \triangleq \alpha_{\text{IRS}} = 2.2$. The small-scale fading is assumed to be the Rayleigh fading. Unless otherwise stated, we set the simulation parameters as follows: Channel bandwidth of 10 MHz, noise power density of -174 dBm/Hz, number of transmit antennas of $N_t = 4$, number of receive antennas of $N_r = 2$, number of data streams of $d = 2$, number of reflection elements of $M = 50$, maximum power of BSs of $P_{l,\text{max}} = 1$ W, $\forall l$, error tolerance of $\varepsilon = 10^{-6}$, and weight factor of $\omega_{l,k} = 1, \forall l, k$. The x coordinate of the center point of the first circle is given by $x_u = 280$ m, which means the users are located at the edge of their corresponding cells. In addition, the location of the IRS is set as $(300, 30)$, which is right above the cell boundary point. The following results are obtained by averaging over 200 independent channel generations. In step 5 of the BCD algorithm, if the MM method is used, the BCD algorithm is denoted as BCD-MM. Similar definition holds for BCD-CCM. The step parameters α and β in the CCM algorithm are set based on Theorem 1.

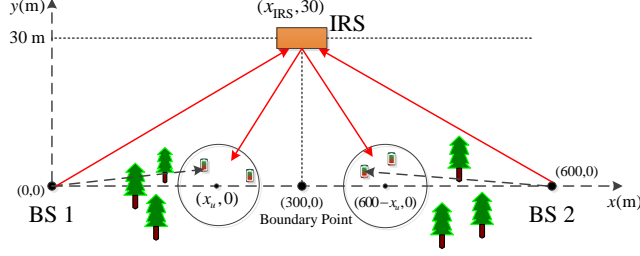


Fig. 3. The simulated two-cell IRS-aided MIMO communication scenario.

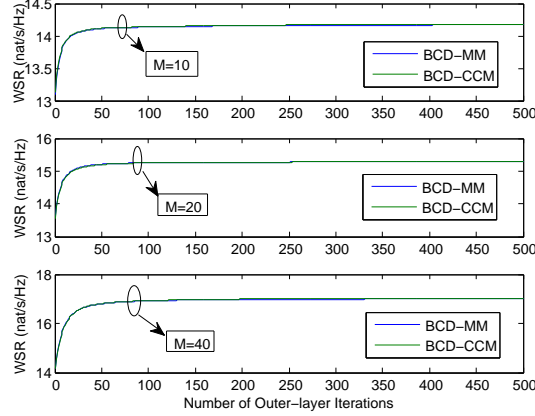


Fig. 4. Convergence behaviour of the BCD algorithm.

A. Properties of the Proposed Algorithms

1) *Convergence Behaviour of BCD Algorithm:* We first study the convergence behaviour of the BCD algorithm in Algorithm 3. Fig. 4 shows the WSR versus the number of iterations for various number of phase shifts, i.e., $M = 10, 20$ and 40 . Two algorithms are tested, i.e., BCD-MM and BCD-CCM. It can be observed from this figure that both BCD-MM and BCD-CCM have a very similar convergence performance in terms of both convergence speed and converged value. More phase shifts leads to a slightly slower convergence speed. This is due to the fact that more optimization variables are involved, and more iterations are needed for convergence. However, for different values of M , the proposed algorithms converge within 100 iterations, which validate the practical implementation of our algorithms.

2) *Convergence behaviour of the MM and CCM algorithms:* In each iteration of the BCD algorithm, we need to use the MM or CCM algorithm to find the phase shifts of the IRS. Fig. 5 shows the convergence performance of the MM and CCM algorithms for the first iteration of the BCD algorithm. It can be seen from Fig. 5 that the MM algorithm converges a little faster than the CCM algorithm, which implies a lower computational complexity of the MM algorithm based

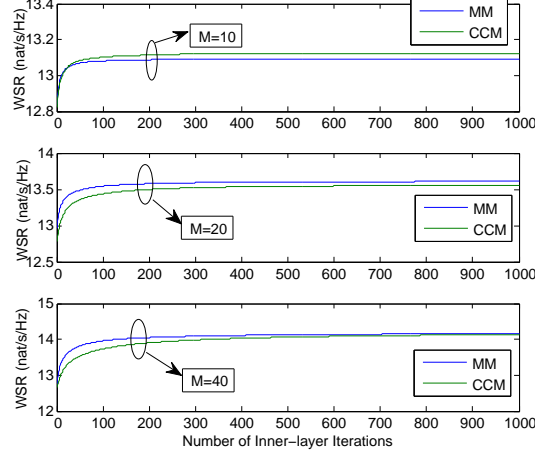


Fig. 5. Convergence behaviour of the MM and CCM algorithm.

on the complexity analysis in Table I. As expected, the number of iterations for convergence of the two algorithms increase with the number of phase shifts since more variables needs to be optimized. For different values of M , the MM algorithm and CCM algorithm may converge to different values. However, as seen from Fig. 4, the final WSR value obtained by the BCD algorithm by using different algorithms to update the phase shifts is almost the same.

B. Performance Comparison

In this subsection, we compare our proposed algorithms with the following benchmark schemes:

- 1) **RandPhase**: We assume that the phase for each reflection element is uniformly and independently generated from $[0, 2\pi]$. We only need to optimize the transmit precoding matrices, which can be obtained by skipping step 5 of the BCD algorithm.
- 2) **No-IRS**: Set the IRS related channel matrices to zero matrices, i.e., $\mathbf{H}_{r,l,k} = \mathbf{0}$, $\mathbf{G}_{n,r} = \mathbf{0}$, $\forall n, l, k$. Then, use the BCD algorithm to find the optimal transmit precoding matrices by removing step 5 for the phase shift update.

1) *Impact of Transmit Power*: Fig. 6 illustrates the average WSR versus the transmit power for various schemes. It can be observed from this figure that the WSR achieved by all the schemes increases with the increase of the transmit power limit. We can also observe that both the BCD-MM algorithm and BCD-CCM algorithm have the similar performance over all ranges of transmit power limit, and both of them significantly outperform the other two benchmark schemes. In addition, the performance gain achieved by the proposed two algorithms over that without the IRS increases with the transmit power limit, which demonstrates the advantages of deploying the

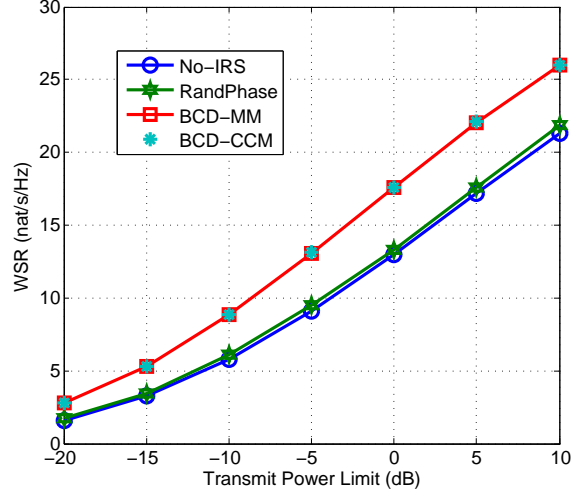


Fig. 6. Achievable WSR versus the transmit power.

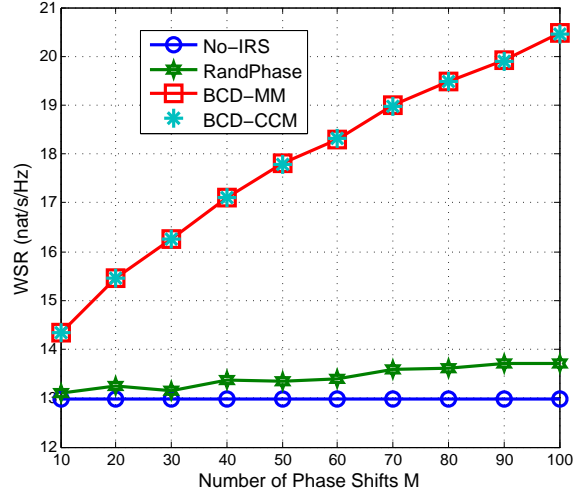


Fig. 7. Achievable WSR versus the number of phase shifts M .

IRS. This is due to the fact that both algorithms can guarantee to converge to a point that is at least locally optimal. It is seen that the performance of the RandPhase algorithm is slightly better than the No-IRS scheme. This is because the reflected signals have not been carefully beamed towards the receive signals. By contrast, for the proposed two algorithms, both the direct signals and reflected signals are superposed more constructively, while the multicell interference signals are added destructively. The IRS can provide more degrees of freedom for optimization, leading to significant performance gains achieved by the proposed algorithms over the RandPhase scheme.

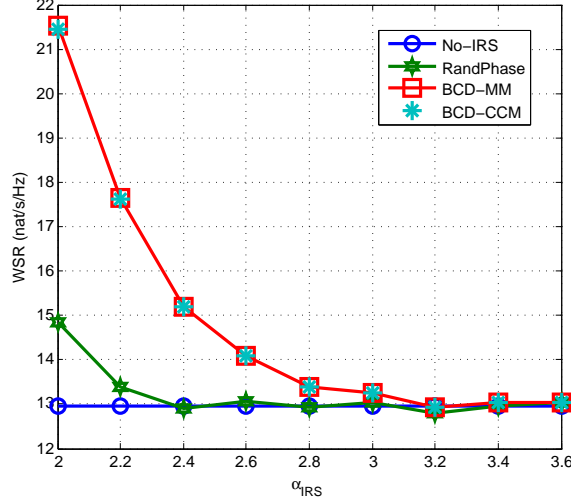


Fig. 8. Achievable WSR versus the IRS-related path loss exponent.

2) *Impact of the Number of Phase Shifts*: Fig. 7 compares the WSR performance of various algorithms versus the number of phase shifts M . It is observed that the WSR achieved by the proposed two algorithms increases with M , and significantly outperforms the other two benchmark algorithms, which keeps almost fixed over the whole range of M . The performance gain becomes pronounced with the increase of M . In specific, when $M = 10$, the performance gain over the No-IRS is only 1.9 bit/s/Hz, while the performance gain increases up to 10.5 bit/s/Hz when $M = 100$. This is mainly attributed to two reasons. First, the received signal power at the IRS can be enhanced by increasing M , leading to a higher array gain. On the other hand, by properly designing the phase shifts, the reflecting signal power received at the users increases accordingly with large M . Hence, the proposed IRS-assisted system can exploit not only the array gain but also the reflecting beamforming gain at the IRS. More importantly, the IRS is a passive reflection device, installing more passive reflecting elements is not only economic-efficient but also energy-efficient since the IRS does not need energy-consuming radio frequency chains and power amplifiers as in conventional transmitters. These results demonstrate that introducing IRS into communications is effective in enhancing the system performance, and is a promising technique for future network.

3) *Impact of the IRS-related Path Loss Exponent*: In the above examples, the path loss exponents of the IRS-related links is set as $\alpha_{\text{IRS}} = 2.2$ since we assume that the location of the IRS can be properly chosen such that free space transmission between BS-IRS link and IRS-user link can be established. However, in some practical scenarios, it may not be able to find such ideal places.

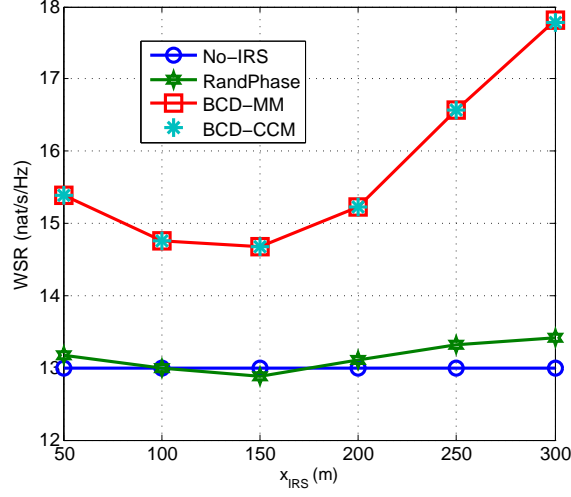


Fig. 9. Achievable WSR versus the location of the IRS x_{IRS} .

Hence, it is intriguing to investigate the performance gain that can be achieved by our proposed algorithms when the IRS-related links experience rich scattering fading with higher value of α_{IRS} . To this end, we plot Fig. 8 to show the impact of the IRS-related path loss exponent. As expected, the WSR achieved by the proposed two algorithms decreases with the increase of α_{IRS} , and finally converges to the same WSR achieved by the No-IRS scheme. The reason is that when increasing α_{IRS} , the signal attenuation associated with the IRS-related links becomes larger, and the received signal from the IRS is weaker and more negligible. However, when α_{IRS} is very small, significant performance gains can be achieved by our proposed algorithms over the No-IRS scheme. For example, for free space channel with $\alpha_{\text{IRS}} = 2$, the performance gain is up to 12.3 bit/s/Hz. Hence, for multicell systems, the performance gain of IRS-assisted systems may be attributed to the favourable channel conditions of the BS-IRS link and IRS-user link. This provides an important engineering design insight where the IRS should be deployed in an obstacle-free scenario such as ceiling for indoor use or advertisement panels for outdoor use. Otherwise, the performance gain brought by the IRS is marginal. Fig. 8 also shows that if the phases shifts are not optimized properly, the performance gain with the IRS may be even worse than that without the IRS, i.e., the WSR achieved by the RandPhase algorithm is equal or lower than that of the No-IRS scheme. This emphasizes the importance of joint optimization of the transmit precoding matrices and the phase shifts at the IRS.

4) *Impact of the IRS Location:* In Fig. 9, we study the impact of the IRS location by moving the IRS from $x_{\text{IRS}} = 50$ m (cell center of the first cell) to $x_{\text{IRS}} = 300$ m (cell boundary). It is again observed that both the proposed algorithms achieve the similar performance, and drastically improves the WSR performance over the other benchmark schemes. It is interesting to observe that the WSR achieved by the proposed algorithms first decrease with x_{IRS} ($50 \text{ m} < x_{\text{IRS}} < 150 \text{ m}$), and then increases with x_{IRS} ($x_{\text{IRS}} > 150 \text{ m}$). This can be roughly explained as follows. Consider a special case where the IRS lies on the line between the BS and the user central point. Denote d as the distance between the BS and the IRS, and D as the distance between the BS and the user central point. By ignoring the small-scale fading, the large-scale channel gain of the combined channel from the IRS is roughly given by

$$\text{PL}_{\text{IRS}} = 2\text{PL}_0 - 10\alpha_{\text{IRS}}\log_{10}(d) - 10\alpha_{\text{IRS}}\log_{10}(D - d). \quad (56)$$

which achieves its minimum value when $d^* = D/2$. Hence, the combined channel gain due to the fact that the IRS achieves its minimum value when the IRS is located at the middle point, which is consistent with the simulation results in Fig. 9. Due to the strong BS-IRS link, the WSR performance gain achieved by our proposed algorithms over the No-IRS is 3.3 bit/s/Hz when $x_{\text{IRS}} = 50$ m. However, this performance gain doubles when the IRS moves to the boundary of these two cells. This performance is not only due to the favourable IRS-user channel link. The other important reason is that we can optimize the phase shifts of the IRS to make the equivalent channel from the inter-cell BS to approach zero matrices. In specific, we can optimize Φ to let $\bar{\mathbf{H}}_{n,l,k}, n \neq l$ approach zero matrices. This can effectively alleviate the severe inter-cell interference for cell-edge users, which significantly enhances the system performance. In addition, deploying the IRS at the cell center for cell 1 is only beneficial for the users in cell 1, while all the users will benefit from the IRS when deploying it at the cell boundary. This means that for multicell communication systems, significant performance gains can be obtained when the IRS is deployed at the cell boundary, which can effectively deal with the inter-cell interference. Furthermore, the phase shifts should be carefully designed. Otherwise, the performance may be inferior to that without IRS, e.g., $x_{\text{IRS}} = 150$ m.

5) *Impact of the User Location:* Finally, we compare the WSR achieved by all schemes versus the horizontal distance between BS 1 and the first circle central point, i.e., x_u . Since users are randomly deployed in this circle, this is equivalent to varying the locations of the users. It is again observed that the proposed two algorithms achieve almost the same performance and achieve

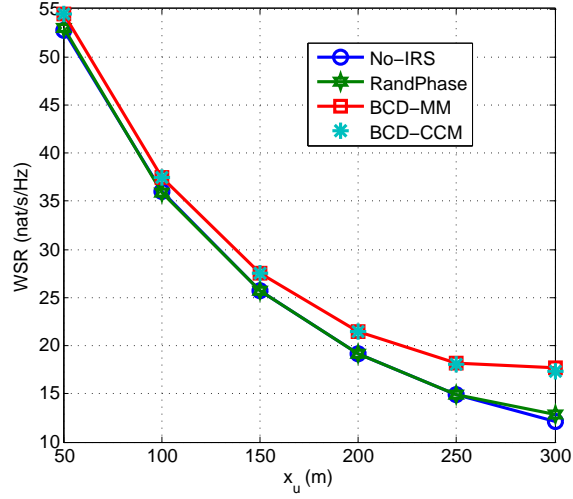


Fig. 10. Achievable WSR versus the location of the first circle central point x_u .

superior performance over the other two benchmark schemes. In addition, the performance gap increases with x_u . The reason is that the users can receive strong reflected signal from the IRS when the users are approaching the cell edge. This means that the IRS is effective in dealing with the inter-cell interference.

V. CONCLUSIONS

In this paper, we proposed to enhance the cell-edge user performance for multicell communication systems by deploying an IRS at the cell boundary. Specifically, by carefully tuning the phase shifts, the inter-cell interference reflected by IRS can be added destructively with that directly from adjacent BSs, which can alleviate the inter-cell interference for cell-edge users. We studied the WSR maximization problem by jointly optimizing the active precoding matrices at BSs and passive shifts at IRS while guaranteeing each BS's power constraint and unit-modulus constraint at the IRS. To tackle this non-convex problem, the BCD algorithm was provided to optimize them in an alternative manner. The optimal precoding matrices can be obtained in closed form, while two efficient algorithms were provided to solve the difficult phase shift optimization problem. Simulation results verify that the proposed algorithms can achieve significant performance gains over the conventional one without incorporating an IRS. Furthermore, the location of IRS should be carefully chosen to guarantee a favourable channel link related to IRS, i.e., BS-IRS link and IRS-user link.

REFERENCES

- [1] W. Zhang, H. Ren, C. Pan, M. Chen, R. C. de Lamare, B. Du, and J. Dai, "Large-scale antenna systems with UL/DL hardware mismatch: Achievable rates analysis and calibration," *IEEE Trans. Commun.*, vol. 63, no. 4, pp. 1216–1229, April 2015.
- [2] J. G. Andrews, S. Buzzi, W. Choi, S. V. Hanly, A. Lozano, A. C. Soong, and J. C. Zhang, "What will 5G be?" *IEEE J. Sel. Areas Commun.*, vol. 32, no. 6, pp. 1065–1082, 2014.
- [3] C. Pan, M. ElKashlan, J. Wang, J. Yuan, and L. Hanzo, "User-centric C-RAN architecture for ultra-dense 5G networks: Challenges and methodologies," *IEEE Commun. Mag.*, vol. 56, no. 6, pp. 14–20, June 2018.
- [4] C. Pan, H. Zhu, N. J. Gomes, and J. Wang, "Joint precoding and RRH selection for user-centric green MIMO C-RAN," *IEEE Trans. Wireless Commun.*, vol. 16, no. 5, pp. 2891–2906, May 2017.
- [5] M. Di Renzo, M. Debbah, D.-T. Phan-Huy, A. Zappone, M.-S. Alouini, C. Yuen, V. Sciancalepore, G. C. Alexandropoulos, J. Hoydis, H. Gacanin *et al.*, "Smart radio environments empowered by reconfigurable AI meta-surfaces: an idea whose time has come," *EURASIP Journal on Wireless Communications and Networking*, vol. 2019, no. 1, p. 129, 2019.
- [6] W. Qingqing and Z. Rui, "Towards smart and reconfigurable environment: Intelligent reflecting surface aided wireless network," *arXiv preprint arXiv:1905.00152*, 2019.
- [7] T. J. Cui, M. Q. Qi, X. Wan, J. Zhao, and Q. Cheng, "Coding metamaterials, digital metamaterials and programmable metamaterials," *Light: Science & Applications*, vol. 3, no. 10, p. e218, 2014.
- [8] O. El Ayach, S. Rajagopal, S. Abu-Surra, Z. Pi, and R. W. Heath, "Spatially sparse precoding in millimeter wave MIMO systems," *IEEE Trans. Wireless Commun.*, vol. 13, no. 3, pp. 1499–1513, 2014.
- [9] X. Yu, J.-C. Shen, J. Zhang, and K. B. Letaief, "Alternating minimization algorithms for hybrid precoding in millimeter wave MIMO systems," *IEEE J. Sel. Topics Signal Process.*, vol. 10, no. 3, pp. 485–500, 2016.
- [10] S. K. Mohammed and E. G. Larsson, "Constant-envelope multi-user precoding for frequency-selective massive MIMO systems," *IEEE Wireless Commun. Lett.*, vol. 2, no. 5, pp. 547–550, October 2013.
- [11] S. K. Mohammed and E. G. Larsson, "Single-user beamforming in large-scale MISO systems with per-antenna constant-envelope constraints: The doughnut channel," *IEEE Trans. Wireless Commun.*, vol. 11, no. 11, pp. 3992–4005, 2012.
- [12] Q. Wu and R. Zhang, "Intelligent reflecting surface enhanced wireless network: Joint active and passive beamforming design," in *2018 IEEE Global Communications Conference (GLOBECOM)*, Dec 2018, pp. 1–6.
- [13] X. Yu, D. Xu, and R. Schober, "MISO wireless communication systems via intelligent reflecting surfaces," *arXiv preprint arXiv:1904.12199*, 2019.
- [14] Y. Yang, B. Zheng, S. Zhang, and R. Zhang, "Intelligent reflecting surface meets OFDM: Protocol design and rate maximization," *arXiv preprint arXiv:1906.09956*, 2019.
- [15] Y. Han, W. Tang, S. Jin, C. Wen, and X. Ma, "Large intelligent surface-assisted wireless communication exploiting statistical CSI," *IEEE Trans. Veh. Technol.*, 2019.
- [16] Q. Wu and R. Zhang, "Intelligent reflecting surface enhanced wireless network via joint active and passive beamforming," *arXiv preprint arXiv:1810.03961*, 2018.
- [17] C. Huang, A. Zappone, G. C. Alexandropoulos, M. Debbah, and C. Yuen, "Reconfigurable intelligent surfaces for energy efficiency in wireless communication," *IEEE Trans. Wireless Commun.*, 2019.
- [18] H. Guo, Y.-C. Liang, J. Chen, and E. G. Larsson, "Weighted sum-rate optimization for intelligent reflecting surface enhanced wireless networks," *arXiv preprint arXiv:1905.07920*, 2019.
- [19] Q.-U.-A. Nadeem, A. Kammoun, A. Chaaban, M. Debbah, and M.-S. Alouini, "Large intelligent surface assisted MIMO communications," *arXiv preprint arXiv:1903.08127*, 2019.

- [20] A. Taha, M. Alrabeiah, and A. Alkhateeb, "Enabling large intelligent surfaces with compressive sensing and deep learning," *arXiv preprint arXiv:1904.10136*, 2019.
- [21] X. Yu, D. Xu, and R. Schober, "Enabling secure wireless communications via intelligent reflecting surfaces," *arXiv preprint arXiv:1904.09573*, 2019.
- [22] M. Cui, G. Zhang, and R. Zhang, "Secure wireless communication via intelligent reflecting surface," *IEEE Wireless Commun. Lett.*, 2019.
- [23] H. Shen, W. Xu, W. Xu, S. Gong, Z. He, and C. Zhao, "Secrecy rate maximization for intelligent reflecting surface assisted multi-antenna communications," *IEEE Commun. Lett.*, pp. 1–1, 2019.
- [24] J. Chen, Y.-C. Liang, Y. Pei, and H. Guo, "Intelligent reflecting surface: A programmable wireless environment for physical layer security," *arXiv preprint arXiv:1905.03689*, 2019.
- [25] D. Gesbert, S. Hanly, H. Huang, S. Shamai Shitz, O. Simeone, and W. Yu, "Multi-cell MIMO cooperative networks: A new look at interference," *IEEE J. Sel. Areas Commun.*, vol. 28, no. 9, pp. 1380–1408, December 2010.
- [26] T. Huang, Y. Yu, and L. Yi, "Design of highly isolated compact antenna array for MIMO applications," *International Journal of Antennas and Propagation*, vol. 2014, 2014.
- [27] C. Pan, H. Zhu, N. J. Gomes, and J. Wang, "Joint precoding and RRH selection for user-centric green MIMO C-RAN," *IEEE Trans. Wireless Commun.*, vol. 16, no. 5, pp. 2891–2906, May 2017.
- [28] M. Grant and S. Boyd, "CVX: Matlab software for disciplined convex programming, version 2.1," 2014.
- [29] X.-D. Zhang, *Matrix analysis and applications*. Cambridge University Press, 2017.
- [30] Y. Sun, P. Babu, and D. P. Palomar, "Majorization-minimization algorithms in signal processing, communications, and machine learning," *IEEE Trans. Signal Process.*, vol. 65, no. 3, pp. 794–816, Feb 2017.
- [31] C. Pan, W. Xu, W. Zhang, J. Wang, H. Ren, and M. Chen, "Weighted sum energy efficiency maximization in ad hoc networks," *IEEE Wireless Commun. Lett.*, vol. 4, no. 3, pp. 233–236, June 2015.
- [32] J. Song, P. Babu, and D. P. Palomar, "Sequence design to minimize the weighted integrated and peak sidelobe levels," *IEEE Trans. Signal Process.*, vol. 64, no. 8, pp. 2051–2064, April 2016.
- [33] K. Alhujaili, V. Monga, and M. Rangaswamy, "Transmit MIMO radar beampattern design via optimization on the complex circle manifold," *IEEE Trans. Signal Process.*, 2019.
- [34] S. Boyd and L. Vandenberghe, *Convex optimization*. Cambridge university press, 2004.